Calculation of Transonic Laminar Flow Airfoils Using a Navier-Stokes Method and Linear Stability Theory

J. Schneider* and B. Ewald†
Technical University of Darmstadt, Germany

Abstract

To study the feasibility of coupling transition prediction by linear stability methods to a Navier-Stokes method, the accuracy of Navier-Stokes mean flow calculations for laminar boundary layers is examined. Navier-Stokes solutions of a flat plate boundary layer are compared to the known Blasius solution. The influence of artificial dissipation level, mesh resolution and mesh stretching is investigated. The severe contamination of the solution by mesh stretching is emphasized. Next, the Navier-Stokes results for a transonic airfoil laminar boundary layer are compared to results from a finite difference boundary layer code. Again, the influence of artificial dissipation level is investigated and shown to be of great influence on solution accuracy. The application of a matrix dissipation model with careful limiter settings yielded the best results. A procedure is described to generate a boundary layer adapted mesh for the airfoil case, based on a Poisson mesh generating procedure. Using the adapted mesh, the accuracy is shown to be greatly improved at no extra computational cost. Finally, Navier-Stokes computations of a transonic laminar airfoil are presented. Here, the transition location is provided by a boundary layer method linked to the Navier-Stokes solution via the pressure distribution.

1 Introduction

To save energy and environmental resources, further drag reduction is a major goal in future transport aircraft design. By achieving partial laminar flow over wing and engine nacelles, a total drag reduction of about 20 percent seems to be possible[1,2], which is quite a strong motivation for increased research effort in this area.

Besides the known great benefit in drag balance, the employment of laminar airfoils also inherits some severe difficulties. On the one hand, there are mechanical problems like, e.g. tolerable surface roughness, integration of de-icing devices and contamination of the leading edge with insects. On the other hand, the airfoil design cycle becomes more difficult since reliable measurements of laminar transonic airfoils at cruise conditions are very expensive. The reason for this is that no Reynolds number scaling by transition tripping can be done, and the testing must be realized at or very near the full scale Reynolds number.

This places emphasis on the theoretical prediction methods. The most general description of the real physics is provided by the Navier-Stokes equations. But also with the efficient and accurate Navier-Stokes solvers available today, the accurate prediction of transonic airfoil performance remains a difficult and challenging task, mainly due to turbulence effects. This is especially true for off-design cases, where strong interactions between the viscous and the convection-dominated parts of the flow occur. Here, the assumption of equilibrium turbulence is no longer valid.

To address this problem, based on the widely used Johnson-King half-equation turbulence model[3], an improved model has been suggested by the present authors[4], which gives better results in weak interaction flows while retaining the ability to predict strongly interacted flows including separation.

When calculating transonic laminar airfoils, the transition location is added to the problem as a new unknown with possible strong influence on the solution. It is therefore necessary to dynamically provide the transition location as the solution converges to steady state. To determine the transition location, several procedures can be chosen, which differ both in accuracy level and computational cost.

There exists a wide variety of empirical transition prediction methods, which however are only valid for a certain type of pressure distribution in the amplification region. In contrast to that, the e^N-method developed independently by Smith[5] and van Ingen[6], doesn't show this restriction and is thus much more generally applicable. Since this method requires a local linear stability analysis of the laminar boundary layer, the Navier-Stokes solution should provide the necessary input for the stability analysis, i.e. velocity and temperature profiles and their first and second derivatives with the required accuracy.

*Research Engineer, Department of Aerodynamics and Measuring Techniques.

†Professor, Department of Aerodynamics and Measuring Techniques.

The computation of local amplification rates and integrated N factors is a task, which requires an appreciable amount of computer time and also needs some user intervention. Since both attributes are not desirable for the use in an iterative computing method, approximative e^N-methods are constructed from a database of precomputed local amplification rates. The latter are usually the result of a linear stability analysis of a laminar similarity (Falkner-Skan) flow. Examples can be found in Refs. 7 – 9. For a given boundary layer, the local amplification rate is then reconstructed from the database via a suitable set of integral coupling parameters, e.g. form parameter H_{12} and displacement thickness Reynolds number Re_{δ_1} for an incompressible case.

The direct stability analysis of a Navier-Stokes solution places the highest demand on the accuracy of the Navier-Stokes-computed velocity and temperature profiles in the boundary layer, since also the first and second derivatives of the profiles are required. The application of database methods slightly alleviates the accuracy problem because of the use of integral parameters. But as clearly shown in Ref. 10, also the computation of these integral parameters is not a trivial task in connection with a Navier-Stokes method. This will be further discussed in this paper.

Besides accuracy, some other problems arise when coupling linear stability analysis to a Navier-Stokes Solver, namely (i) identification of the boundary layer, and (ii) backward shift of the transition location into the turbulent region. To solve the first problem, a method was suggested by the present authors[11], which will be briefly summarized in the next section. The second problem will arise, if up to the last found transition location no amplified mode with a critical N factor could be found and thus the analysis had to be continued inside the turbulent region.

When using a boundary layer method to completely generate all input to the stability analysis, all of these coupling problems vanish since the only link between Navier-Stokes solution and stability analysis is the Navier-Stokes pressure distribution. On the other hand, this method of course exhibits minimum integration of the transition calculation into the Navier-Stokes method.

2 Identification of the boundary layer

In a Navier-Stokes method, the identification of the boundary layer, i.e. the finding of the boundary layer edge, is not trivial. This is due to the recursive definition of the boundary layer thickness δ. Assuming constant total enthalpy together with the isentropic relation outside the boundary layer allows the computation of the boundary layer edge velocity U_e from the wall pressure p_w. Unfortunately, small total pressure variations in the Navier-Stokes solution and the above mentioned assumptions make it infeasible to use this U_e for the determination of the boundary layer edge.

Using the approach of Stock and Haase[12] for turbulent boundary layers as a starting point, a similar method was developed in Ref. 11 for laminar boundary layers. The boundary layer thickness is found to be in a constant relation to the wall distance of the maximum of a function f_{lam}, where

$$f_{\text{lam}} = y^{\alpha}\frac{\partial u}{\partial y}, \qquad \alpha = 4.755.$$

Now, the boundary layer thickness is given by

$$\delta_{\text{lam}} = 1.486\, y_{\max}, \tag{1a}$$

$$y_{\max} = y\,(f_{\text{lam}} = \max)\,. \tag{1b}$$

Figure 1 displays the function f_{lam} computed from solutions of the Falkner-Skan equation for different pressure gradient parameters m, showing the location of the maxima to be independent of m. More quantitative information is provided

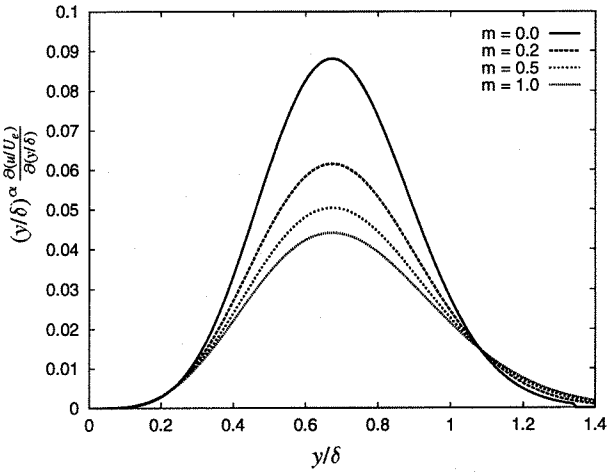

Figure 1: Function $f = (y/\delta)^{\alpha}\,\partial(u/U_e)/\partial(y/\delta)$ for different pressure gradient parameters m

by *figure 2*, which shows the loci $(y/\delta)_{\max}$ for 106 different pressure gradient parameters m, ranging from $m = -0.09$ (separation) to $m = 1$ (stagnation flow). The $(y/\delta)_{\max}$ values are essentially constant in the positive m range, with some deviation to larger values in the negative m region.

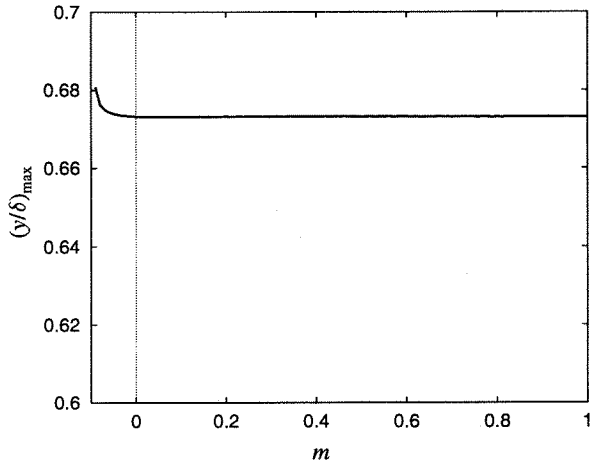

Figure 2: Location $(y/\delta)_{\max}$ for a range of pressure gradient parameters m, using $\alpha = 4.755$

3 Numerical methods

Navier-Stokes method

The Reynolds averaged Navier-Stokes equations are solved with the finite-volume, cell centered, block-structured Navier-Stokes code ENSSO[13, 14]. The code uses central differencing spatial discretisation and consequently needs artificial dissipation to assure stability. Since the artificial dissipation is of particular interest when computing laminar boundary layers, the flux formulation will be described briefly. At the interface between two cells i and $i+1$, the modified flux reads

$$\boldsymbol{F}_\xi := \boldsymbol{F}_\xi\left(\frac{1}{2}(\boldsymbol{U}_{i,j} + \boldsymbol{U}_{i+1,j})\right) + \boldsymbol{D}_\xi, \tag{2}$$

where $\boldsymbol{U}$ is the vector of conservation variables, and $\boldsymbol{D}_\xi$ is the artificial dissipative flux in ξ direction. $\boldsymbol{D}_\xi$ is a blend of second and fourth order differences[15]:

$$\boldsymbol{D}_\xi = (D_\xi^2 - D_\xi^4)\boldsymbol{U}_{i,j}.$$

The second and fourth order differences are given by[16]

$$\begin{aligned} D_\xi^2 &= |\boldsymbol{A}|\varepsilon_2\Delta_{i,j}\boldsymbol{U}_{i,j} \\ D_\xi^4 &= |\boldsymbol{A}|\varepsilon_4\Delta_{i,j}\nabla_{i,j}\Delta_{i+,j}\boldsymbol{U}_{i,j}, \end{aligned}$$

Where Δ and ∇ are forward and backward difference operators, respectively. The parameters ε_2 and ε_4 control the switching between second and fourth order dissipation:

$$\varepsilon_2 = \kappa_2 \max(\nu_{i-1,j}, \nu_{i,j}, \nu_{i+1,j}, \nu_{i+2,j}) \tag{3a}$$

$$\varepsilon_4 = \max\left(0, (\kappa_4 - \alpha\varepsilon_2)\right), \tag{3b}$$

with ν being a shock sensing function[15]. The default setting for κ_2 and κ_4 is 1/2 and 1/64, respectively. This can be changed by user input. $|\boldsymbol{A}|$ is the absolute value of the flux Jacobian given by

$$|\boldsymbol{A}| = \boldsymbol{T}|\boldsymbol{\lambda}|\boldsymbol{T}^{-1},$$

where $|\boldsymbol{\lambda}|$ is the diagonal matrix of the absolute eigenvalues of $\boldsymbol{A}$, $\boldsymbol{T}$ and $\boldsymbol{T}^{-1}$ are the matrices of the right and left eigenvectors of $\boldsymbol{A}$, respectively. Using this formulation for $|\boldsymbol{A}|$, a matrix dissipation model is constructed. The eigenvalues for the ξ direction are given by

$$\begin{aligned} \lambda_1 &= (y_\eta u - x_\eta v) + c\sqrt{x_\eta^2 + y_\eta^2} \\ \lambda_2 &= (y_\eta u - x_\eta v) - c\sqrt{x_\eta^2 + y_\eta^2} \\ \lambda_3 &= (y_\eta u - x_\eta v) = \lambda_4 \end{aligned}$$

Since the linear eigenvalues $\lambda_3 = \lambda_4$ vanish at stagnation points and under certain situations of grid alignment with the flow, and the nonlinear eigenvalues may vanish at sonic points, a limiter must be introduced in the following way:

$$\begin{aligned} |\lambda_1| &:= \max(|\lambda_1|, l_n\rho) \\ |\lambda_2| &:= \max(|\lambda_2|, l_n\rho) \\ |\lambda_3| &:= \max(|\lambda_3|, l_l\rho), \end{aligned}$$

where ρ is the spectral radius (maximum eigenvalue) of $\boldsymbol{A}$. The default values are $l_n = l_l = 0.4$. As we will show later, improved accuracy can be achieved by reducing the linear eigenvalue limiter for the η (normal to the wall) direction to $l_{l,\eta} = 0.1$. In the ξ direction the default value of $l_{l,\xi} = 0.4$ must be retained for stable convergence.

When $|\boldsymbol{A}|$ is replaced by the spectral radius of $\boldsymbol{A}$, a scalar dissipation model is established, as suggested in Ref. 15.

Grid generation

Grids are generated with the recently developed code GRID2D[17] by solving the Poisson equations for the curvilinear coordinates ξ, η:

$$\Delta\xi_i = P_i, \qquad i = 1, 2. \tag{4}$$

The source terms P_i are used to control the mesh spacing. To be solved in the physical domain, the system (4) must be transformed to the x, y coordinate system:

$$g_{22}(\vec{x}_{\xi\xi} + P_1'\vec{x}_\xi) + g_{11}(\vec{x}_{\eta\eta} + P_2'\vec{x}_\eta) - 2g_{12}\vec{x}_{\xi\eta} = 0, \tag{5}$$

where g_{ij} are the elements of the covariant metric tensor, while P_1' and P_2' are given by $P_1' = \frac{gP_1}{g_{22}}$ and $P_2' = \frac{gP_2}{g_{11}}$, respectively. Here, g is the determinant of the metric tensor. The transformed system (5) can be inverted to obtain the source terms P_i', which would be required to generate a given mesh:

$$\begin{bmatrix} P_1' \\ P_2' \end{bmatrix} = \frac{1}{\sqrt{g}}\boldsymbol{M}\begin{bmatrix} 2g_{12}x_{\xi\eta} - g_{22}x_{\xi\xi} - g_{11}x_{\eta\eta} \\ 2g_{12}y_{\xi\eta} - g_{22}y_{\xi\xi} - g_{11}y_{\eta\eta} \end{bmatrix}, \tag{6a}$$

where

$$\boldsymbol{M} = \begin{bmatrix} g_{11}y_\eta & -g_{11}x_\eta \\ -g_{22}y_\xi & g_{22}x_\xi \end{bmatrix}. \tag{6b}$$

By fixing the metric coefficients to some desired values, the source terms determined by eqs. (6) can be used to iteratively drive the generated mesh to this fixed metric. Consider the problem of generating a boundary orthogonal mesh with prescribed point distribution along the boundary together with prescribed distance of the first mesh line from the boundary. In this case, $g_{12} = 0$ (orthogonality), while $g_{11} = \Delta s_{(\xi)}^2$ and $g_{22} = \Delta s_{(\eta)}^2$ are known from the prescribed mesh spacing tangential and normal to the boundary. Additionally, the derivatives normal to the boundary are computed using mirror cells also representing the required local metric.

This approach is used in GRID2D to generate boundary-orthogonal meshes controlling the distance of the first mesh line and the boundary point locations prescribed by user input. As discussed later, this method can also be used to generate boundary layer adapted meshes.

4 Accuracy of the Navier-Stokes solution

The accuracy of Navier-Stokes solutions in laminar boundary layers is a problem recently addressed by several

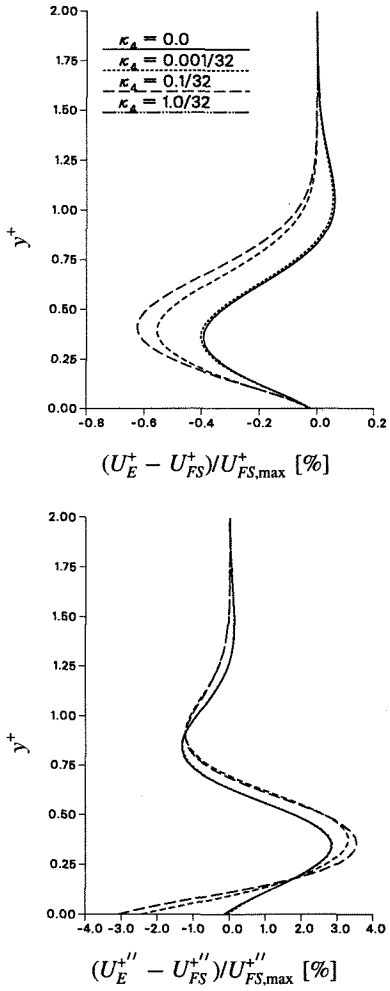

Figure 3a: Influence of artificial dissipation level on solution error. Mesh consists of 64 equidistributed cells, 32 in the boundary layer. Above: velocity, below: second derivative of velocity.

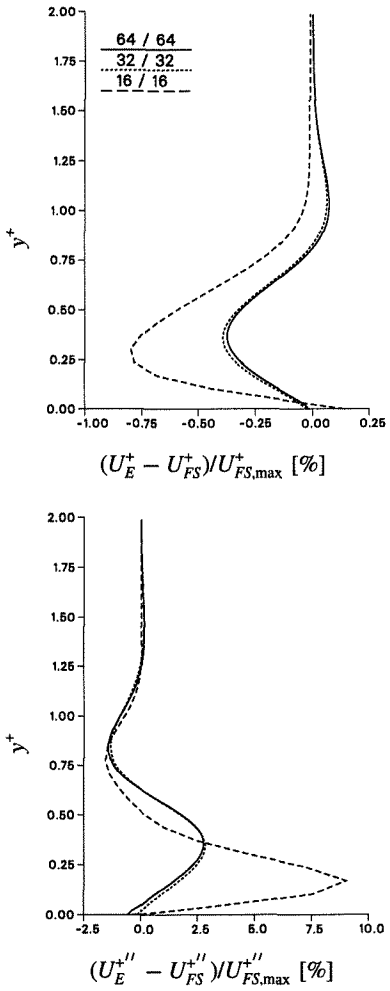

Figure 3b: Influence of mesh resolution on solution error, $\kappa_2 = \kappa_4 = 0$. The legend denotes the number of cells inside / outside of the boundary layer. Above: velocity, below: second derivative of velocity.

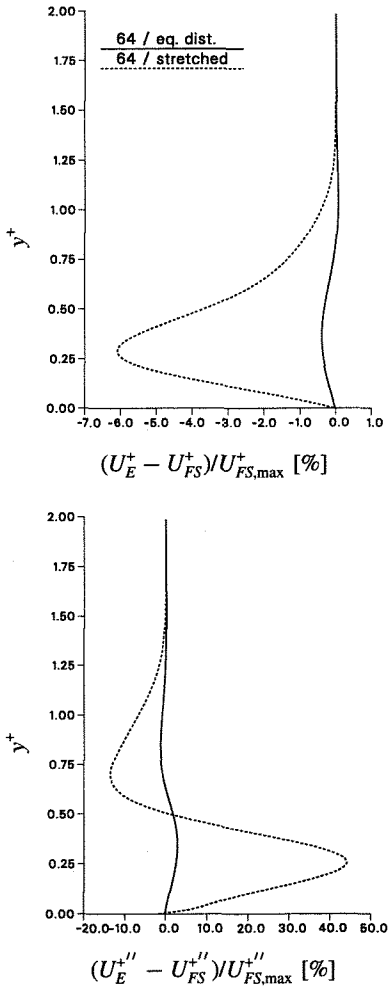

Figure 3c: Influence of mesh stretching on solution error, $\kappa_2 = \kappa_4 = 0$. Above: velocity, below: second derivative of velocity.

authors[18–20]. It was pointed out by Swanson and Turkel[18], that, in conjunction with a central differencing spatial approximation, a matrix dissipation model is essential for improved accuracy, especially when calculating high-*Re* flows.

Flat plate boundary layer cases

In Ref. 11, the present authors have investigated Navier-Stokes solutions for a flat plate boundary layer with respect to the influence of artificial dissipation level, mesh resolution, and mesh stretching. The flow was computed for $9 \cdot 10^4 \leq Re_x \leq 2 \cdot 10^6$. The free stream Mach number was taken to be $M_\infty = 0.4$. *Figure 3* shows the Navier-Stokes solution error with respect to a Falkner-Skan (Blasius) solution. To compare the results, non-dimensional errors against the Blasius-Solution are plotted. Here, the non-dimensional quantities

$$u^+ = \frac{u}{U_e}, \quad \text{and} \quad y^+ = \frac{y}{\delta}$$

are used. The ENSSO Navier-Stokes solution is denoted by the subscript E and the Blasius (Falkner-Skan) solution by the subscript FS.

The influence of scalar artificial dissipation level is displayed in *figure 3a*. The mesh consists of 64 equidistributed cells, 32 in the boundary layer. Since for this case, stable convergence to steady state could be obtained with no artificial viscosity at all, i.e. $\kappa_2 = 0$ and $\kappa_4 = 0$ in eqs. (3), an artificial dissipation free solution can be taken as reference. In all cases, $\kappa_2 = 0$. A very small value of $\kappa_4 = 0.1/32$, which would be clearly too low for other flow fields, already shows significant deviation to the $\kappa_4 = 0$ case.

Figure 3b shows a series of computations with 16 / 32 / 64 cells in the boundary layer. Dissipation settings were $\kappa_4 = \kappa_2 = 0$. The 64 cells case achieves no significant

improvement over the 32 cells case. The remaining deviations with respect to the Blasius solution are mainly due to compressibility effects present at $M = 0.4$.

Probably most interesting with respect to "real" airfoil flows is *figure 3c*, which shows the influence of mesh stretching in normal direction. Again, $\kappa_4 = \kappa_2 = 0$. The mesh consisted of a total of 64 cells in normal direction, with a moderate stretching factor of 1.03 being applied in this direction. For the stretched mesh, the error is increased by a factor of 16 to 20. Since in the present Navier-Stokes method, the fluxes across the cell faces are computed using simple arithmetic averaging of the conservation variables, see eq. (2), in regions of high solution gradients every cell stretching in the gradient direction leads to severe discretisation errors. This must be kept in mind when generating meshes for laminar airfoil cases.

In Ref. 11, a Navier-Stokes solution of a flat plate boundary layer flow using $\kappa_4 = 0.1/32$ and 35 equally distributed cells in the boundary layer, was analyzed with the compressible stability analyzer COAST2[21]. The results are compared to a stability calculation using the Blasius solution together with the known flat plate boundary layer development $\delta = \delta_0\sqrt{x/x_0}$. The N factors calculated from the Navier-Stokes solution were very close to the N factors from the Blasius solution, showing the feasibility of a direct stability analysis of the Navier-Stokes solution despite the errors seen in *figure 3*.

Airfoil cases

For linear stability analysis of transonic laminar airfoil flows, the accuracy of the corresponding Navier-Stokes solution must be investigated. In Ref. 10, this was carried out with regard to mesh resolution, using scalar artificial dissipation. Unfortunately, no information was provided in Ref. 10 regarding the values of the dissipation coefficients κ_2 and κ_4. It was stated there, that the mesh resolution must be very high (about 60 to 70 cells in the boundary layer, as compared with 20 to 30 for normal airfoil cases) to produce sufficient accuracy. In the present work, emphasis is placed on the influence of the artificial dissipation level and on sophisticated mesh generation to reduce the required number of cells in the boundary layer.

The investigations are carried out for the RAE 2822 airfoil, using free stream parameters corresponding to case 9 of Ref. 22. The mesh shows C type topology and consists of 304 cells in tangential and 64 cells in normal direction. 208 cells are located on the airfoil and 30 cells inside the boundary layer, with estimated boundary layer thicknesses of $\delta = 0.001c$ at the leading edge and $\delta = 0.04c$ at the trailing edge. In normal direction, the grid spacing follows a geometric progression with different stretching factors inside and outside the boundary layer. The distance of the first mesh line is chosen in a way, that would resolve the viscous sublayer in a turbulent boundary layer. The far field boundary is located at a distance of about 10 chords from the airfoil surface. *Figure 4* shows the mesh and a cut-out

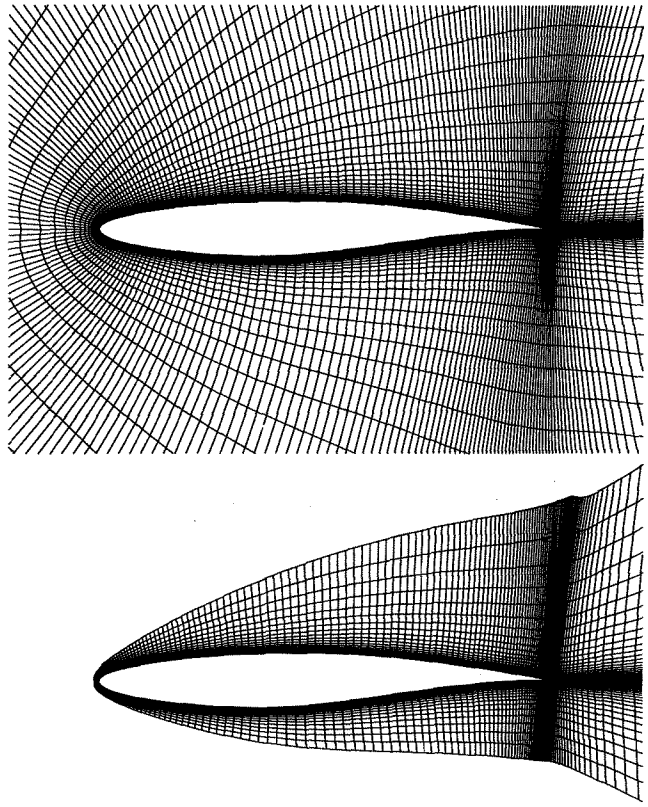

Figure 4: Original mesh for the airfoil cases. Cutout of the first 30 cells is blown up in η-direction by a factor of 10.

of the first 30 cells normal to the wall, which is blown up in η-direction by a factor of ten to make things more visible. *Figure 5* shows the pressure distribution for the investigated airfoil case.

Transition is fixed to $0.45c$ on upper and lower side. To investigate the accuracy of the Navier-Stokes solution in a laminar boundary layer, the form parameter H_{32} is compared to a solution generated by a compressible finite-difference boundary layer code[23] using the Navier-Stokes pressure distribution. For the finite-difference code solutions, the boundary layer was resolved using approximately 100 points. Momentum and energy thickness were computed by

$$\delta_2 = \int_0^\delta \frac{\rho U}{\rho_e U_e}\left(1 - \frac{U}{U_e}\right) \mathrm{d}y$$

$$\delta_3 = \int_0^\delta \frac{\rho U}{\rho_e U_e}\left(1 - \left(\frac{U}{U_e}\right)^2\right) \mathrm{d}y,$$

respectively. *Figure 6* shows a series of computations with successively lower artificial dissipation level using the scalar dissipation model. The accuracy of the laminar boundary layer computation is strongly affected by the artificial dissipation level, while the turbulent part shows considerable

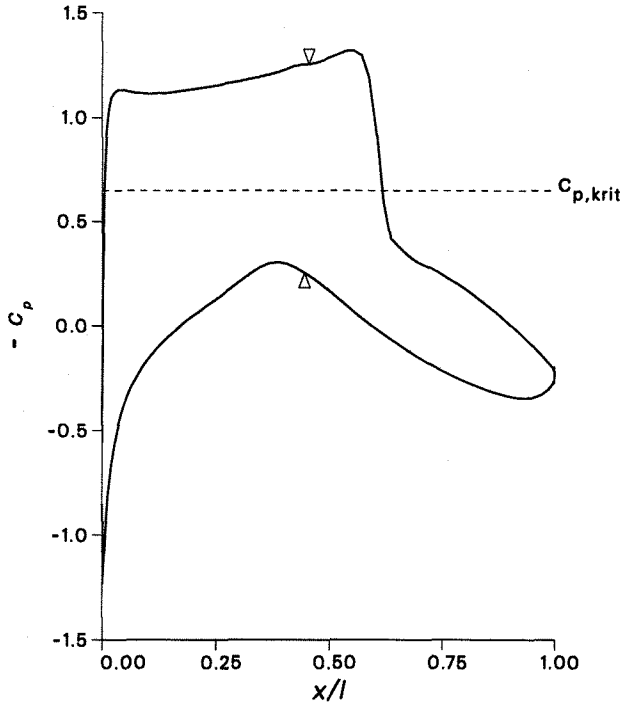

Figure 5: Pressure distribution for the investigated airfoil cases. Triangles denote transition locations.

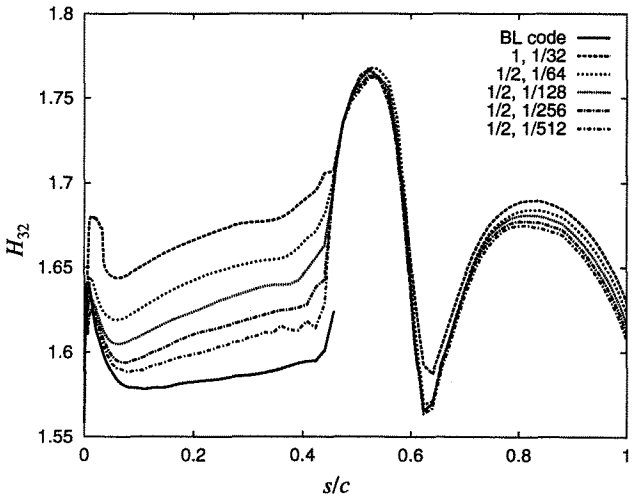

Figure 6: Influence of scalar artificial dissipation level on solution accuracy. First number denotes the value of κ_2, second number the value of κ_4.

less contamination due to the much higher level of physical dissipation in a turbulent boundary layer. The lowest filter level of $\kappa_2 = 1/2$, $\kappa_4 = 1/512$ already shows some convergence problems, which is also manifested in the oscillations in front of the transition point.

Using the matrix dissipation model and the standard values of $\kappa_2 = 1/2$ and $\kappa_4 = 1/64$, the results presented in *figure 7* are obtained. As mentioned earlier, the limiter for the linear eigenvalues should be set to different values for the ξ and the η direction. Using a value of $l_{l,\eta} = 0.1$ shows a distinct improvement over the default value of $l_{l,\eta} = 0.4$.

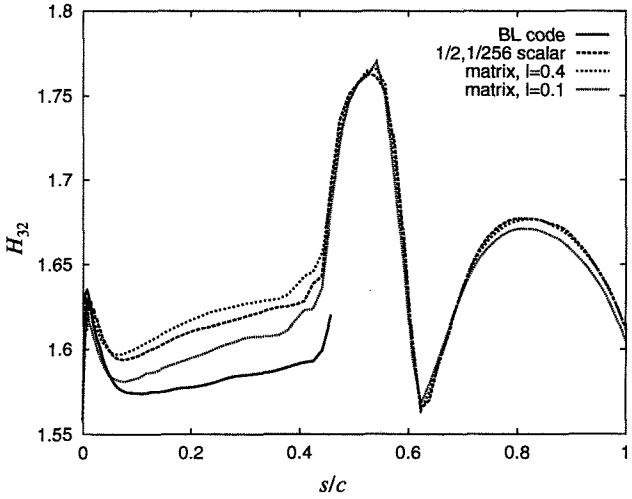

Figure 7: Comparison of scalar and matrix dissipation model using different values for the linear limiter $l_{l,\eta}$

For comparison, the result from the scalar dissipation model using the lowest κ_4 value showing stable convergence, is also plotted in *figure 7*. Obviously, for the matrix dissipation model to be superior to the scalar model, the limiter values have to be carefully adjusted to the computed case.

The H_{32} values achieved using the matrix dissipation model and $l_{l,\eta} = 0.1$, seem to represent the most accurate solution possible on the present mesh. The remaining deviations with respect to the finite difference code solution can only be reduced by increasing the number of cells in normal direction or by better distribution of the mesh lines while keeping their total number constant. The latter approach will be applied here. This is done in a five step process.

In the first step, the location of the boundary layer edge is determined using relation (1) for the laminar part and the Stock-Haase[12] relation for the turbulent boundary layer. In the "transition" region near the point, where the turbulence model is switched on, a special treatment is necessary, which is detailed in Ref. 11.

The second is the determination of the local distance of the first mesh line from the boundary, $\Delta s_{(\eta)0}$. For this, the friction velocity $u_\tau = \sqrt{(\tau_w/\rho_w)}$ is chosen as a scaling parameter:

$$\Delta s_{(\eta)0} = y_0^+ \frac{\nu}{u_\tau}, \tag{7}$$

where ν is the kinematic viscosity. The parameter y_0^+ is set to a value of $y_0^+ = 1$ for the present calculations. Using (7), the distance of the first mesh line is controlled by the local wall shear and is thus larger in laminar regions and smaller in turbulent ones. Hence, the necessary mesh stretching in the laminar region can be reduced. Additionally, proper resolution of the viscous sublayer in turbulent boundary layers is assured.

In the third step, the mesh points are redistributed in normal η direction using δ from step one, $\Delta s_{(\eta)0}$ from step two, and a prescribed number of cells in the boundary layer. This

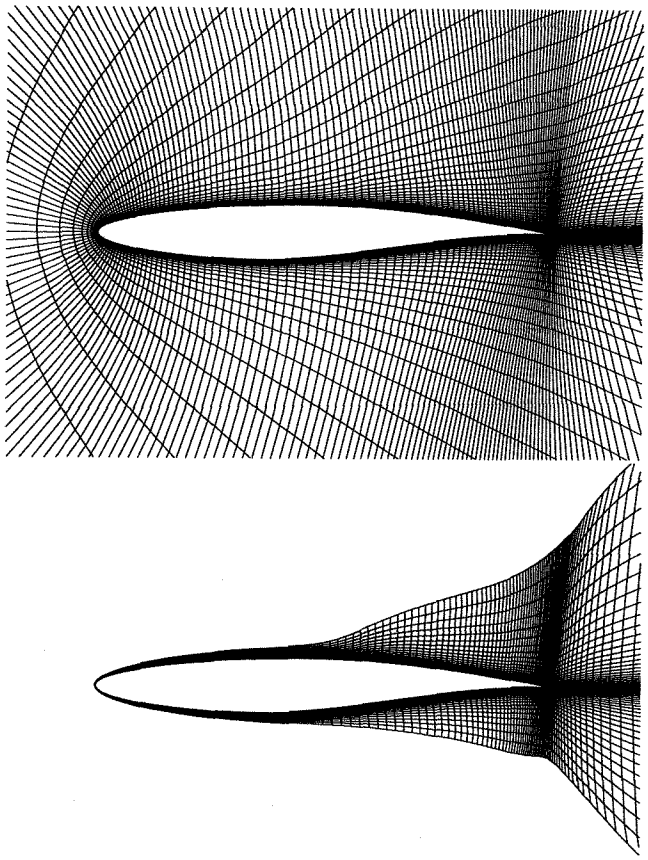

Figure 8: Adapted mesh for the airfoil cases. Lower figure shows the mesh covering the boundary layer (30 cells) with coordinates in η-direction blown up by a factor of 10.

is performed by a geometric stretching function with different constant factors inside and outside the boundary layer, which ensures a smooth grid transition over the boundary layer edge.

Since this algebraic mesh generation procedure has the unwanted property of propagating disturbances like e.g., local change in $\Delta s_{(\eta)0}$, through the whole mesh, in a fourth and fifth step, the mesh is regenerated inside and outside the boundary layer, respectively, using the Poisson system (5). To calculate the appropriate source terms for the Poisson system, the approach described earlier is chosen: after applying step three, the local metric, i.e. g_{ij}, at the wall and at the boundary layer edge is stored and then used in eq. (6). For each η grid line, the source terms P'_2, which control the spacing in η direction, are set to the value of P'_2 at the wall for the inner mesh and to the value of P'_2 at the boundary layer edge for the outer mesh, respectively. Any other procedure, e.g. interpolation to some different value at the other edge of the η line, yielded unsatisfactory results. The source terms P'_1 are kept from the initial mesh.

Figure 8 shows the adapted mesh and a blow-up of its boundary layer part. The number of cells in the boundary layer was set to 30, according to the results from the flat

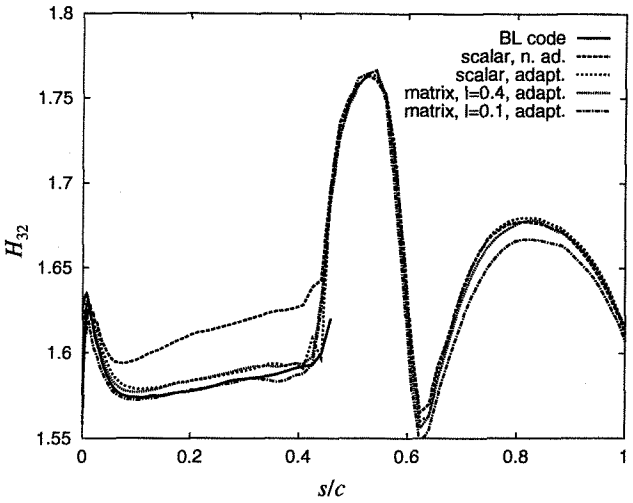

Figure 9: Comparison of adapted vs. non-adapted mesh. Scalar cases use $\kappa_2 = 1/2$, $\kappa_4 = 1/256$, while matrix cases use $\kappa_2 = 1/2$, $\kappa_4 = 1/64$.

plate cases. This is also the number of cells used for the estimated boundary layer of the non-adapted mesh.

Navier-Stokes results obtained by using the adapted mesh are compared to the boundary layer code results in *figure 9*. The scalar dissipation results use $\kappa_2 = 1/2$, $\kappa_4 = 1/256$, while the matrix dissipation uses $\kappa_2 = 1/2$, $\kappa_4 = 1/64$. Generally, the accuracy level is greatly improved upon the non-adapted case, which is shown for comparison. Again, the limiter value of $l_{l,\eta} = 0.1$ performs better than $l_{l,\eta} = 0.4$. The scalar dissipation result shows some oscillation at the onset of transition. In contrast to the non-adapted cases, the differences between the various dissipation levels are reduced on the adapted mesh.

It must be kept in mind, that this improvement was obtained without increasing the total number of cells in the coordinate mesh, and thus without increasing the computational cost. This is in contrast to the findings in Ref. 10, where the total number of cells in normal direction is at least doubled over the present value of 30, to achieve the required accuray.

5 Transonic laminar airfoil computations

While the direct stability analysis of a Navier-Stokes solution represents the closest possible coupling, it also exhibits some severe problems regarding the accuracy of the Navier-Stokes solution, as discussed above. Moreover, the stability analysis itself may be problematic, both in computing cost and necessary user intervention.

The next level of integration would be given by applying a database stability method, see Ref. 7, to predict the transition location. Here, the Navier-Stokes solution accuracy problem is also present, but can be resolved with tolerable computation costs, as described in the previous section.

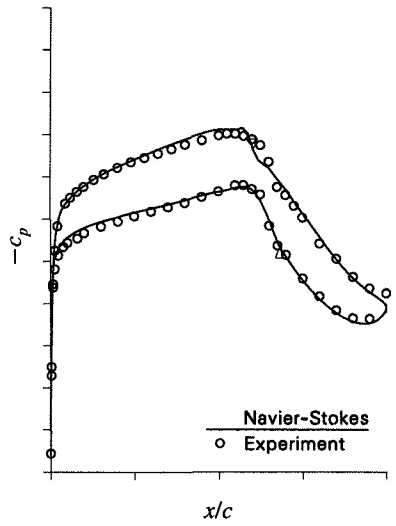

Figure 10a: Pressure distribution for $M = 0.74$, $Re = 6 \cdot 10^6$, $\alpha_M = 0.495°$, $\alpha_{comp} = -0.064°$. Triangles denote transition locations.

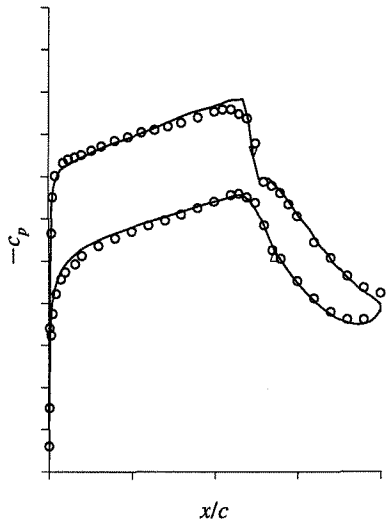

Figure 10b: Pressure distribution for $M = 0.74$, $Re = 6 \cdot 10^6$, $\alpha_M = 1.499°$, $\alpha_{comp} = 0.655°$.

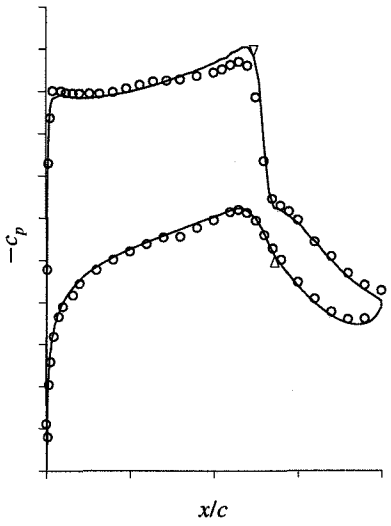

Figure 10c: Pressure distribution for $M = 0.74$, $Re = 6 \cdot 10^6$, $\alpha_M = 3.006°$, $\alpha_{comp} = 1.976°$.

However, the question of a suitable continuation of the stability analysis into the turbulent region is still present, see Ref. 10.

An alternate approach is to provide the input to the stability analysis by means of a boundary layer method, which is linked to the Navier-Stokes solution via the pressure distribution. The boundary layer method can provide the required accuracy level with less effort than the Navier-Stokes method. Additionally, the problem of shifting the transition location backwards into the turbulent region does not arise.

The integral two-equation boundary layer method of Drela and Giles[9] provides an integrated approximative e^N method, which uses an empirical function $dN/dRe_{\delta_2} = f(H_{12})$. This relation is constructed from a database of precomputed amplification rates for a range of solutions to the Falkner-Skan equation. For every pressure gradient parameter m, the N factor envelope over a range of frequencies is approximated by a linear relation, giving one discrete point of the above mentioned empirical function.

Applying this alternate approach, the boundary layer method of Ref. 9 was implemented into the Navier-Stokes code ENSSO. At certain stages during the convergence process (every 5 multigrid cycles on the finest mesh in the computations presented here), the boundary layer method is called with the current Navier-Stokes wall pressure distribution. For upper and lower side, it computes an arc length measured from stagnation point, at which transition occurs. This is then translated to cell indices in the Navier-Stokes mesh, at which the turbulence model is switched on.

Figure 10 shows pressure distributions of a laminar transonic airfoil computed with this procedure. The agreement with measured data[24] is fairly good, though the measured data experiences some wind tunnel wall effects. In all cases, convergence of the interacted problem turns out to be very stable.

6 Conclusions

The ability of a finite-volume Navier-Stokes method to accurately predict laminar boundary layers was examined.

The influence of artificial dissipation level, mesh resolution and mesh stretching on the solution error was studied using a flat plate boundary layer. Especially mesh stretching in the main gradient direction (normal to the wall) is shown to dramatically contaminate the Navier-Stokes solution. Resolution of the boundary layer with approximately 30 (equidistributed) cells seems to yield sufficient accuracy.

For a transonic airfoil case, Navier-Stokes solutions were compared to solutions by a finite-difference boundary layer code. In the laminar portion of the boundary layer, the artificial dissipation level has a strong effect on the Navier-Stokes solution, as opposed to the turbulent region, where the effect is nearly negligible. Application of a matrix dissipation model using a reduced value of the linear eigenvalue limiter for the η direction, yielded the most accurate results. On the other hand, the standard scalar dissipation model with reduced values of the fourth order dissipation parameter κ_4, also showed sufficient accuracy, with CPU times reduced by approximately 15 percent as compared to the matrix dissipation.

To compute Navier-Stokes results in close agreement with boundary layer code results, either an increased number of mesh points in the normal direction must be used, or the mesh must be carefully adapted to the laminar boundary layer. Applying the second approach, a five step method is presented to generate a boundary-layer-adapted mesh, which uses a Poisson mesh generation procedure. The results obtained with this mesh are greatly improved upon the non-adapted mesh while using the same total number of mesh points. Interestingly, the differences between the different artificial dissipation levels are also reduced on the adapted mesh.

Direct stability analysis of the Navier-Stokes solution seems to be the most straightforward approach, as inside the framework of linear stability theory, no further simplifications have to be made. Also, the extension to 3D problems should easily be possible. On the other hand, the accuracy level needed for direct stability analysis requires a highly resolved laminar boundary layer, thereby increasing the computational costs, and a very careful treatment of the dissipative fluxes, thereby increasing the requirements for spatial discretisation and/or artificial dissipation formulation. Additionally, direct stability analysis causes high computational costs, and automatic processing without user intervention is not easily possible. In all cases, where the input to the linear stability method is generated by a Navier-Stokes method, the problem of backward shifting the transition location into the turbulent region is present.

As an alternate approach, an integral boundary layer method, which includes an approximate e^N-method, is implemented in the Navier-Stokes code. Here, the only link between transition prediction and Navier-Stokes method is the pressure distribution. This interaction scheme greatly improves convergence stability as compared to the method presented in Ref. 10. Some results are presented for a transonic laminar airfoil, which show good agreement to the experiment.

7 Acknowledgment

The authors are grateful to G. Dargel of Deutsche Airbus Bremen, for providing the experimental data for the transonic laminar airfoil case.

References

[1] Horstmann, K. H., Köster, H., Quast, A., and Redeker, G.: Laminarprofile für Verkehrsflugzeuge. IB 129-85/12, DFVLR, 1985.

[2] Szodruch, J.: Airbus and the Technological Challenge of the Next Ten Years. In Szodruch, J., (Ed.), *Technological Developments for Commercial Transport Aircraft*: Airbus Industrie, Blagnac, 1993.

[3] Johnson, D. A. and King, L. S.: A Mathematically Simple Turbulence Closure Model for Attached and Separated Turbulent Boundary Layers. *AIAA J.*, Vol. 23 (No. 11), pp. 1684–1692, Nov. 1985.

[4] Schneider, J. and Ewald, B.: Ein verbessertes Ungleichgewichts-Turbulenzmodell für transsonische Profilströmungen. DGLR 93-03-051, DGLR-Jahrestagung, 1993.

[5] Smith, A. M. O. and Gamberoni, N.: Transition, Pressure Gradient and Stability Theory. Rept. ES 26388, Douglas Aircraft Company, Long Beach, CA, 1957.

[6] van Ingen, J. L.: A suggested Semi-Empirical Method for the Calculation of the Boundary Layer Transition Region. Rept. VTH-74, Dept. of Aerospace Engineering, Delft, Nederlande, 1956.

[7] Stock, H. W. and Degenhart, E.: A simplified e^n method for transition prediction in two-dimensional, incompressible boundary layers. *Z. Flugwiss. Weltraumforsch.*, Vol. 13, pp. 16 – 30, 1989.

[8] Dini, P., Selig, M. S., and Maughmer, M. D.: Simplified Linear Stability Transition Prediction Method for Separated Boundary Layers. *AIAA J.*, Vol. 30 (No. 8), pp. 1953 – 1961, 1992.

[9] Drela, M. and Giles, M. B.: Viscous-Inviscid Analysis of Transonic and Low Reynolds Number Airfoils. *AIAA J.*, Vol. 25 (No. 10), pp. 1346 – 1355, 1987.

[10] Radespiel, R., Graage, K., and Brodersen, O.: Transition Predictions Using Reynolds-Averaged Navier-Stokes and Linear Stability Analysis Methods. AIAA Paper 91-1641, 1991.

[11] Schneider, J. and Ewald, B.: Integration of Linear Stability Methods into Navier-Stokes Solvers for Computation of Transonic Laminar Airfoils. AIAA Paper 94-1849, 1994.

[12] Stock, H. W. and Haase, W.: The Determination of Turbulent Length Scales in Algebraic Turbulence Models for Attached and Slightly Seperated Flows Using Navier-Stokes Methods. AIAA Paper 87-1302, 1987.

[13] Lieser, J. A.: *Theoretische und experimentelle Untersuchungen transsonischer Heckströmungen.* Dissertation, Technische Hochschule Darmstadt, 1992.

[14] Reimann, J. and Schneider, J.: ENSSO — An Efficient 2D Finite-Volume Multigrid Navier-Stokes Solver for Block-Structured Configurations. Bericht A 123/93, TH Darmstadt, Aerodynamik und Meßtechnik, 1993.

[15] Jameson, A., Schmidt, W., and Turkel, E.: Numerical Solutions of the Euler Equations by Finite Volume Methods Using Runge-Kutta Time-Stepping Schemes. AIAA Paper 81-1259, 1981.

[16] Swanson, R. C. and Turkel, E.: On Central Difference and Upwind Schemes. *J. of Comput. Physics*, Vol. 101 (No. 2), 1992.

[17] Schneider, J.: Ein Programm zur algebraischen und elliptischen Netzgenerierung für beliebige 2D-blockstrukturierte Netze. Bericht A 88/91, TH Darmstadt, Aerodynamik und Meßtechnik, 1991.

[18] Swanson, R. and Turkel, E.: Aspects of a High-Resolution Scheme for the Navier-Stokes Equations. AIAA Paper 93-3372, 1993.

[19] Ramakrishnan, R., Vatsa, V., Otto, J., and Kumar, A.: A Detailed Study of Mean-Flow Solutions for Stability Analysis of Transitional Flows. AIAA Paper 93-3052, 1993.

[20] Garriz, J. A., Vatsa, V. N., and Sanetrik, M. D.: Issues Involved in Coupling Navier-Stokes Mean-Flow and Linear Stability Codes. AIAA Paper 94-0304, 1994.

[21] Schrauf, G.: An efficient solver for the eigenvalue problem of the linear stability equations for three-dimensional, compressible boundary layer flows. 6. DGLR-Fach-Symposium „Strömungen mit Ablösung", 08. – 10. Nov. 1988 in Braunschweig, 1988.

[22] Cook, P. H., McDonald, M. A., and Firmin, M. C. P.: Aerofoil RAE 2822 — Pressure Distributions, Boundary Layer and Wake Measurements. AR 138, AGARD, 1979.

[23] Cebeci, T. and Bradshaw, P.: *Physical and computational aspects of convective heat transfer.* Springer, New York Berlin Heidelberg, 1988.

[24] Dargel, G. Private communication, 1994.